Contents lists available at ScienceDirect

Chemical Engineering Research and Design

journal homepage: www.elsevier.com/locate/cherd

An analytical method for the optimization of pore network in lithium-ion battery electrodes

*Guanghua Ye, Weiwen Tong, Xinlei Liu, Xinkuan Song, Jinghong Zhou, Xinggui Zhou**

State Key Laboratory of Chemical Engineering, East China University of Science and Technology, Shanghai 200237, China

ARTICLE INFO

Article history:
Received 2 April 2019
Received in revised form 19 June 2019
Accepted 28 June 2019
Available online 17 July 2019

Keywords:
Analytical method
Optimization
Pore network structure
Lithium-ion battery
Electrode
Tortuosity

ABSTRACT

Engineering the hierarchical pore network structure is one effective way to improve the lithium-ion battery electrodes without changing their materials chemistry. Herein, a simple yet powerful analytical method is developed to design the electrode with the hierarchical pore network. In this method, the analytical expression of the effective tortuosity is obtained as the objective function, which can well reflect the electrode performance. This method is validated in two limiting cases and one case between the two limiting cases, through comparing the analytical results with the numerical ones calculated by the Newman model. Employing this method, the electrode with the hierarchical pore network is optimized at different total porosities and electrode thicknesses. The optimal electrode with the hierarchical pore network shows up to 350% improvement in the energy density at 5C rate, when comparing to the conventional electrode. The analytical method in this work provides a useful tool for the optimization of the lithium-ion battery electrodes.

1. Introduction

Lithium-ion batteries are widely used in portable electronics as energy storage devices, due to their high energy/power densities and long life compared to conventional batteries, like zinc-manganese battery. To use lithium-ion batteries in large-scale applications, such as hybrid and electric vehicles, further improvements in energy and power densities are required (Etacheri et al., 2011). One effective way to achieve these improvements is developing new electrode materials, in which great progress has been made in recent years (Kang and Ceder, 2009; Nitta et al., 2015; Palacín, 2009); another approach is designing the pore network structure of electrodes without changing the materials chemistry (Bae et al., 2013; Billaud et al., 2016), which can also greatly improve the batteries but receives much less attention.

In a porous electrode of lithium-ion batteries, ion transport can be the rate-limiting step during charge and discharge, especially at high rates (Cobb and Blanco, 2014; Miranda et al., 2016). The strong ion transport limitation can cause significant concentration polarization and capacity loss, which greatly reduce energy and power densities. This ion transport resistance is primarily determined by the pore network structure of the electrode with specific electrode materials and electrolyte. For example, the size of active particles strongly affects the Li-ion insertion/extraction kinetics (Park et al., 2010); the thickness and porosity of an electrode have great influences on Li-ion diffusion through the electrode (Cobb and Blanco, 2014; Dai and Srinivasan, 2016). Therefore, it is necessary to optimize the pore network structure of the electrodes.

The benefits of optimizing lithium-ion battery electrodes have been reported in the literature. For instance, Fuller et al. (1994) and Srinivasan and Newman, (2004) optimized carbon/manganese dioxide and carbon/iron phosphate lithium-ion cells. They found a thinner electrode with more porosity is favorable at a faster discharge due to the reduced ion transport limitation, while a thicker electrode with less porosity is preferable at a slower discharge because of the decreased volume fraction of inert materials (e.g., current collectors and separators). Doyle and Fuentes, (2003) improved a commercial lithium-ion polymer cell by increasing the mass ratio of cathode to anode active materials and the thicknesses of the electrodes. The new design achieves the significant increases of capacity from 520 to 680 mAh and energy density from 124 to 171 Wh/kg, but at the expense of the slight losses in specific power and cycle life. Ramadesigan et al. (2010) and Golmon et al. (2014) improved electrodes by spatially varying porosity, and they observed the significant reduction in ion transport resistance and improvement in discharge capacity. Recently, Dai and Srinivasan, (2016) further

* *Corresponding author.*
E-mail address: xgzhou@ecust.edu.cn (X. Zhou).
https://doi.org/10.1016/j.cherd.2019.06.038

explored the influence of the graded electrode porosity, and they found the electrode performance can be improved only in the base cases far from the optimum. They also claimed that judiciously using a constant porosity can lead to a similar improvement and spatially varying porosity shows only a marginal improvement in energy density. The similar results about the spatial distribution of porosity can also be found in the optimization of catalysts and adsorbents (Rao and Coppens, 2010; Wang et al., 2007; Ye et al., 2015).

In the aforementioned works, the lithium-ion batteries have a conventional sandwich structure, and the optimum is the trade-off between power and energy densities. However, both improvements in power and energy densities are required to meet the ever-growing energy storage demands. Except developing new electrode materials and electrolytes, there are still some approaches to achieve the improvements in power and energy densities simultaneously. One approach is devising three-dimensional (3D) battery architectures, such as 3D-interdigitated and 3D-trench geometries (Long et al., 2004; Pikul et al., 2013). In 3D batteries, the external surface area of electrodes is increased, and the Li-ion transport path is shorten. But, 3D batteries are still far from commercialization, since their large-scale manufacture is difficult and costly. Another approach is introducing low-tortuosity pore channels into a conventional electrode as "high-way" for ion transport, which results in a hierarchical pore network (Bae et al., 2013). This approach does not change the conventional sandwich structure of lithium-ion batteries, and thus is very promising for large-scale applications. Besides, hierarchical pore networks are also widely adopted in biology, such as trees crowns and lungs (Coppens and Ye, 2018). In biology, to meet the challenge of transporting nutrients toward cells and products (including waste) away from cells through multiple length scales, using hierarchical pore network becomes the choice for most animals and plants after billions of years of evolution. Inspired by this, an optimized hierarchical pore network could significantly improve the electrode performance.

Several attempts have been made to fabricate the electrodes with additional pore channels perpendicular to current collectors, and the simultaneous improvements in power and energy densities have been observed in experiments. For instance, Bae et al. (2013) and Sander et al. (2016) introduced these low-tortuosity pore channels into lithium cobalt oxide cathodes using the methods of co-extrusion and magnetic templating, and they observed a 200% improvement in the area capacity at a practical charge-discharge rate. Billaud et al. (2016) fabricated the graphite anode with graphite flakes perpendicular to the current collector using an external magnetic field, and the specific charge of the magnetically aligned anode is 3 times higher than that fabricated in a conventional route at a rate of 1C. Although much progress in manufacturing technologies is still required to produce electrodes with hierarchical pore networks on a large scale and at a low cost, engineering hierarchical pore networks provides an effective way to simultaneously improve power and energy densities. In order to guide the rational design of the hierarchical pore network in the electrodes, it is essential to develop a proper optimization method.

At present, the numerical method based on the Newman model (Doyle et al., 1993) has been used to optimize the hierarchical pore network in lithium-ion battery electrodes. Cobb and Blanco, (2014) numerically optimized the lithium cobalt oxide cathode with a hierarchical pore network, and they reported that the preferred width of electrode pillars is 25–100 μm for the ultra-thick electrode on the order of 150–300 μm. However, the numerical optimization method usually gives the optimum at a particular location, and it is computationally intensive for multi-objective, multi-variable optimizations (Subramanian and White, 2000). An analytical optimization method is more general and requires much less computational cost, and thus it is preferable for the optimization of the hierarchical pore network that is complex and involves many structural variables. For conventional electrodes, the analytical solutions of current density, ion concentration, specific energy, and specific power have been derived with some simplifications of the Newman model (Doyle and Newman, 1997; Newman, 1995; Subramanian and White, 2000). For the electrode with a hierarchical pore network, a proper analytical optimization method has not been reported in the literature to the best of our knowledge.

In this work, an analytical method is developed to optimize the lithium-ion battery electrode with a hierarchical pore network. This analytical optimization method is validated in three archetypical cases, through comparing the analytical results with the numerical ones obtained from the Newman model. By using this method, the widths of the low-tortuosity pore channels and electrode pillars are optimized with different total porosities and electrode thicknesses.

2. Methodology

2.1. Hierarchical pore network

The typical lithium-ion battery electrode with a hierarchical transport network is illustrated in Fig. 1a–c, and this type of hierarchical pore system is also employed in catalysis and adsorption (Schwieger et al., 2016). Hierarchical transport networks are widely adopted in biology to meet the similar challenge of transporting mass, and one example is shown in Fig. 1d. The cuboid pore channels perpendicular to the current collector are introduced into the electrode as the fast transport routes, and the tortuous pores in the electrode pillars provide slow transport routes but large internal surface area for electrochemical reactions. Fig. 1b displays the two dimensional geometry of a repeating unit of the electrode. The width of the electrode pillars is w_e, the width of the pore channels is w_p, and the thickness of the electrode coating is h. This electrode geometry is simple and representative, and it is adequate to reflect the general features of hierarchical pore networks. Besides, for other electrode geometries, their structural optimization is more complex and computationally more expensive. Therefore, in this work, the analytical optimization method is developed based on the electrode geometry in Fig. 1.

2.2. Analytical expression of effective tortuosity

For a conventional electrode, its tortuosity, τ, can be defined as (Hutzenlaub et al., 2013):

$$\tau = \varepsilon \frac{D}{D_e} \tag{1}$$

where ε is the porosity; D is the intrinsic diffusion coefficient of lithium-ion that is measured in the electrolyte without the confinement of pores; D_e is the effective diffusion coefficient of lithium-ion that includes the effect of porous structure of electrodes. Eq. (1) indicates that the tortuosity is the only geometric parameter that affects the electrode performance, when the porosity and thickness of the electrode coating are constant. Therefore, the analytical expression of effective tortuosity can be utilized to optimize the hierarchical pore network in the electrode.

The tortuosity of a cuboid pore channel is 1 (the minimum value of tortuosity), while the tortuosity of the pore network in an electrode pillar can be much larger than 1. To obtain the effective tortuosity of the electrode with the hierarchical pore network, we assume a pseudo-homogeneous electrode where the pseudo-homogeneous description of diffusivity, porosity, tortuosity, and many other macroscopic properties is employed. This pseudo-homogeneous electrode has the same total porosity and coating thickness as the electrode with the hierarchical pore network, and the effective concentration drops of the two electrodes are also the same. In this way, the tortuosity of the pseudo-homogeneous electrode is assumed to be the effective tortuosity of the electrode with the hierarchical pore network.

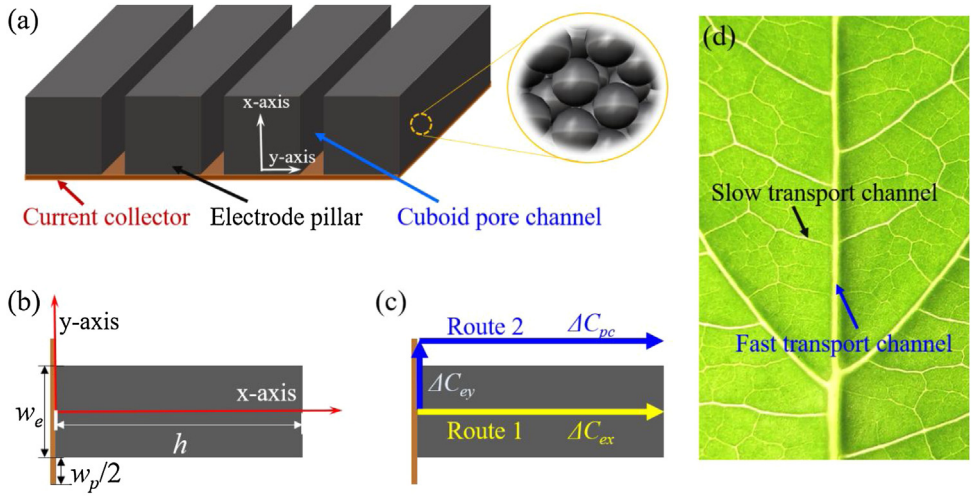

Fig. 1 – (a) An illustration of the lithium-ion battery electrode with additional cuboid pore channels perpendicular to the current collector; (b) the two-dimensional geometry of a repeating unit of the electrode and its structural parameters; (c) ion transport routes and their associated concentration drops; (d) the hierarchical pore network in a leaf. Δc_{ex} is the concentration drop in the electrode pillar along the x direction, Δc_{pc} is the concentration drop in the pore channel, and Δc_{ey} is the concentration drop in the electrode pillar along the y direction.

In the pseudo-homogeneous electrode, the concentration drop can be obtained by analytically solving the mass balance equation:

$$\varepsilon\frac{\partial c}{\partial t} = \frac{\varepsilon}{\tau_{eff}}D\frac{\partial^2 c}{\partial x^2} + aj_n(1-t_+^0) \tag{2}$$

where c is the concentration of lithium ion, t is the time, x is the thickness of the electrode coating from the current collector, τ_{eff} is the effective tortuosity, a is the specific interfacial area of the electrode coating, j_n is the pore wall flux of lithium ions, and t_+^0 is the transference number of lithium ion that is constant. To simplify the derivation of the concentration drop, the steady state equation is used and the uniform electrochemical reaction rate through the electrode is assumed (Doyle and Newman, 1997; Fuller et al., 1994; Richardson et al., 2012; Zhang and White, 2007):

$$0 = \frac{\varepsilon}{\tau_{eff}}D\frac{\partial^2 c}{\partial x^2} + aj_n(1-t_+^0) \tag{3}$$

$$aj_n = -\frac{I}{Fh} \tag{4}$$

where I is the superficial current density and F is the Faraday's constant. The boundary conditions for Eq. (3) are:

$$\frac{\partial c}{\partial x} = 0 at x = 0 \tag{5}$$

$$c = c_b at x = h \tag{6}$$

where c_b is the concentration of lithium ion at $x = h$. Analytically solving Eqs. (3)–(6), we obtain the concentration drop of the pseudo-homogeneous electrode (Δc_p):

$$\Delta c_p = \tau_{eff}\frac{I(1-t_+^0)h}{2F\varepsilon D} \tag{7}$$

Eq. (7) indicates the concentration drop is independent on c_b, which validates the use of steady state equation. It is worth noting that the assumption of uniform electrochemical reaction rate is reasonable when the open circuit potential is strongly dependent on the state of charge or kinetic resistances dominate ohmic resistances (Doyle and Newman, 1997; Fuller et al., 1994; Richardson et al., 2012). Besides, the analytical method proposed in this work may not be suitable for the cases where the assumption of uniform electrochemical reaction rate breaks down.

In the electrode with cuboid pore channels, there are two ion transport routes (see Fig. 1c): (1) one dimensional diffusion through the electrode pillar; (2) lateral diffusion through the electrode pillar and then transport through the cuboid pore channel. Accordingly, there are three concentration drops. The overall concentration drop of the electrode with the hierarchical pore network (Δc_h) is obtained by mimicking the addition of parallel resistors:

$$\Delta c_h = \left(\frac{1}{\Delta c_{ex}} + \frac{1}{\Delta c_{pc} + \Delta c_{ey}}\right)^{-1} \tag{8}$$

The mass balance equations in the electrode pillar (Eq. (9)) and cuboid pore channel (Eq. (10)) are:

$$0 = \frac{\varepsilon_e}{\tau_e}D\left(\frac{\partial^2 c}{\partial x^2} + \frac{\partial^2 c}{\partial y^2}\right) + a_e j_n(1-t_+^0) \tag{9}$$

$$0 = D\left(\frac{\partial^2 c}{\partial x^2} + \frac{\partial^2 c}{\partial y^2}\right) \tag{10}$$

where ε_e, τ_e and a_e are the porosity, tortuosity and specific surface area of the electrode pillar. The tortuosity can be calculated by $\tau_e = \varepsilon_e^{1-m}$ where m is the Bruggeman porosity exponent (Hutzenlaub et al., 2013). It is worth noting that there are negligible diffusion barriers between cuboid pore channels and narrow pores of electrode pillars, as cuboid pore channels and narrow pores are not significantly different in size and the diffusion behaviors in the two types of pores are similar (Bae et al., 2013; Cobb and Blanco, 2014; Lueth et al., 2016). The porosity ε_e and specific surface area a_e are related to the

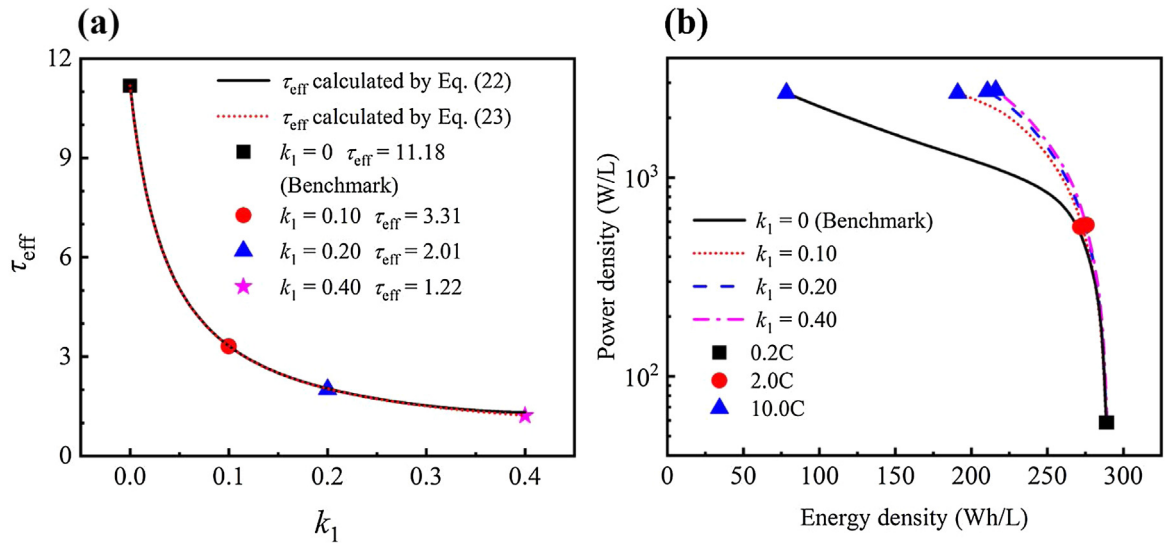

Fig. 2 – Validation of the analytical method in case 1 ($k_2 = 0.01$). (a) The relation between k_1 and the effective tortuosity; (b) the Ragone plots at $k_1 = 0$, 0.1, 0.2 and 0.4. Simulation parameters: $h = 60$ μm, $\varepsilon = 0.35$, the other parameters are given in Table S1 in the Supplementary Information.

widths of the electrode pillar and cuboid pore channel, when the total porosity (ε) is constant:

$$\varepsilon_e = \varepsilon + (\varepsilon - 1)\frac{w_p}{w_e} \tag{11}$$

$$a_e = \left(1 + \frac{w_p}{w_e}\right) a \tag{12}$$

To obtain the concentration drop in the electrode pillar along the x direction Δc_{ex}, Eq. (9) is simplified to:

$$0 = \varepsilon_e^m D\frac{\partial^2 c}{\partial x^2} + a_e j_n(1 - t_+^0) \tag{13}$$

The boundary conditions for Eq. (13) are the same to Eqs. (5) and (6). The solution of Eqs. (13), (5), and (6) yields the concentration drop in the electrode pillar along the x direction:

$$\Delta c_{ex} = \frac{I(1 - t_+^0)}{2FD\varepsilon_e^m}\left(1 + \frac{w_p}{w_e}\right) h \tag{14}$$

To acquire the concentration drop in the cuboid pore channel, Eq. (10) can be approximated by:

$$0 = D\frac{\partial^2 c}{\partial x^2} + a_e j_n(1 - t_+^0)\frac{w_e}{w_p} \tag{15}$$

where the reaction current term represents the lithium ions generated in electrode pillars and then diffused along the y direction into cuboid pore channels. The boundary conditions for Eq. (15) are the same to Eqs. (5) and (6). Solving Eqs. (15), (5), and (6), we obtain the concentration drop in the pore channel:

$$\Delta c_{pc} = \frac{I(1 - t_+^0)}{2FD}\left(1 + \frac{w_e}{w_p}\right) h \tag{16}$$

To acquire the concentration drop in the electrode pillar along the y direction, Eq. (9) is approximated by:

$$0 = \varepsilon_e^m D\frac{d^2 c}{dy^2} + a_e j_n(1 - t_+^0) \tag{17}$$

The boundary conditions of Eq. (17) are:

$$\frac{\partial c}{\partial y} = 0 \, at \, y = 0 \tag{18}$$

$$c = c_p \, at \, y = \frac{w_e}{2} \tag{19}$$

where c_p is the concentration of lithium ion in the cuboid pore channel. Analytically solving Eqs. (17)–(19) gives the concentration drop in the electrode pillar along the y direction:

$$\Delta c_{ey} = \frac{I(1 - t_+^0)}{8FD\varepsilon_e^m}\left(1 + \frac{w_p}{w_e}\right)\frac{w_e^2}{h^2} h \tag{20}$$

Nominating $k_1 = \frac{w_p}{w_e}$ and $k_2 = \frac{w_e}{h}$, and then substituting Eqs. (14), (16), and (20) into Eq. (8), the overall concentration drop of the electrode with the hierarchical pore network is:

$$\Delta c_h = \frac{I(1 - t_+^0)h}{2FD}\left[\frac{1}{1 + \frac{1}{k_1} + \frac{1}{4\varepsilon_e^m}(1 + k_1)k_2^2} + \frac{\varepsilon_e^m}{1 + k_1}\right]^{-1} \tag{21}$$

Equaling Eqs. (7) and (21), we obtain the effective tortuosity:

$$\tau_{eff} = \varepsilon\left[\frac{1}{1 + \frac{1}{k_1} + \frac{1}{4\varepsilon_e^m}(1 + k_1)k_2^2} + \frac{\varepsilon_e^m}{1 + k_1}\right]^{-1} \tag{22}$$

2.3. *Optimization*

The effective tortuosity (Eq. (22)) can be the objective function when the total porosity and thickness of the electrode are fixed, as the effective tortuosity is the only geometric variable that affects the electrode performance. By minimizing

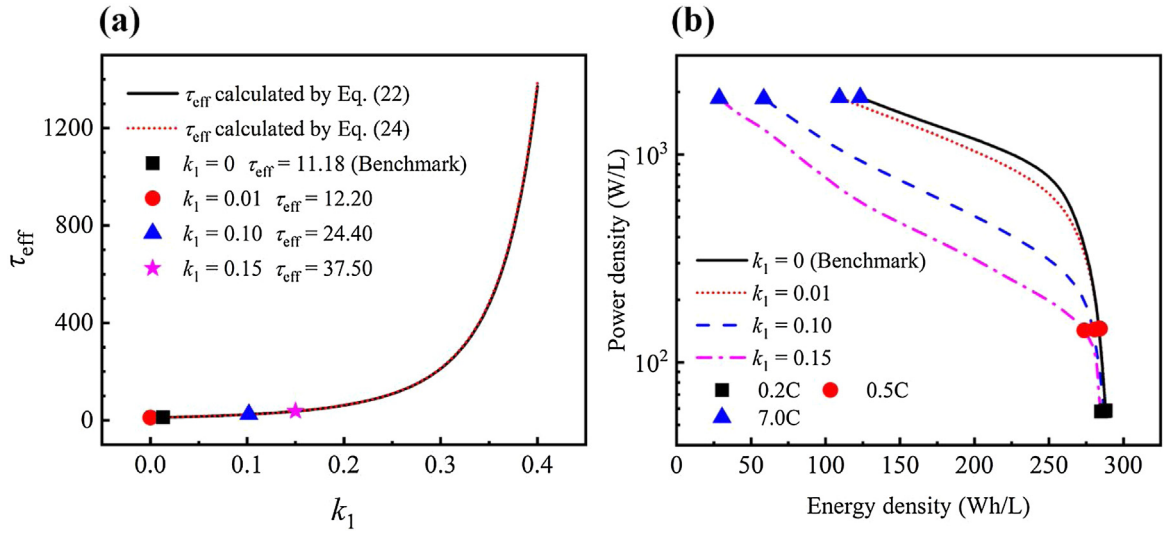

Fig. 3 – Validation of the analytical method in case 2 ($k_2 = 20$). (a) The relation between k_1 and the effective tortuosity; (b) the Ragone plots at $k_1 = 0$, 0.01, 0.1 and 0.15. Simulation parameters: $h = 60$ μm, $\varepsilon = 0.35$, the other parameters are given in Table S1 in the Supplementary Information.

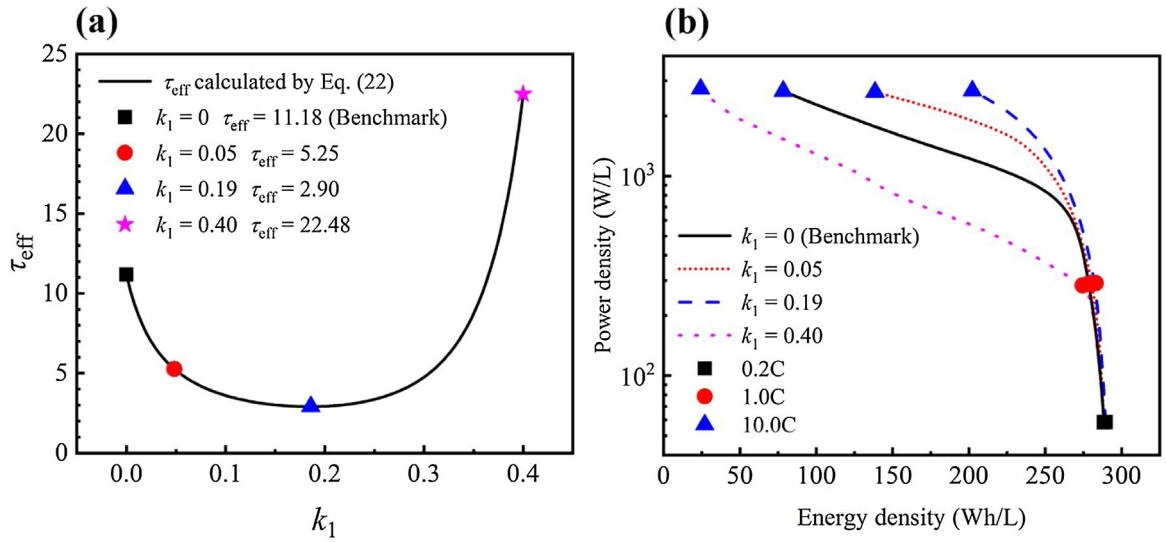

Fig. 4 – Validation of the analytical method in case 3 ($k_2 = 0.25$). (a) The relation between k_1 and the effective tortuosity; (b) the Ragone plots at $k_1 = 0$, 0.05, 0.19 and 0.4. Simulation parameters: $h = 60$ μm, $\varepsilon = 0.35$, the other parameters are given in Table S1 in the Supplementary Information.

this effective tortuosity, the optimal widths of the electrode pillar and cuboid pore channel can be obtained.

To validate and apply this analytical method, we take the anode of a commercial lithium-ion battery (UP 383562, Sony) as an example. A cell of this commercial lithium-ion battery consists of graphite anode, $LiPF_6$ in ethylene carbonate (EC)/propylene carbonate (PC) electrolyte, porous polyethylene separator, Cu and Al foils, and $LiCoO_2$ cathode. The anode of this cell has the hierarchical pore network (see Fig. 1), while the other parts keep unchanged. The analytical results are compared with the numerical ones calculated by a pseudo two-dimensional model based on the Newman model (Doyle et al., 1993). The simulation parameters are taken from the literature (Doyle and Fuentes, 2003), and they are summarized in Table S1 in the Supplementary Information. The numerical simulations are implemented in COMSOL Multiphysics (COMSOL Inc., version 4.3), and the finite element method is used to discretize the spatial domains. These numerical simulations can well predict the experiments reported in the literature (Doyle and Fuentes, 2003), as shown in Fig. S1 in the Supplementary Information. Therefore, the numerical simulations can provide accurate power and energy densities, which can be used to validate the analytical method.

3. Results and discussion

3.1. *Method validation*

The analytical method proposed in this work is validated in three typical cases: two limiting cases (case 1 and case 2) and a case between the limiting cases (case 3). In case 1, the width of the electrode pillar or the ratio between the width and the thickness of the electrode pillar (k_2) is very small, and the

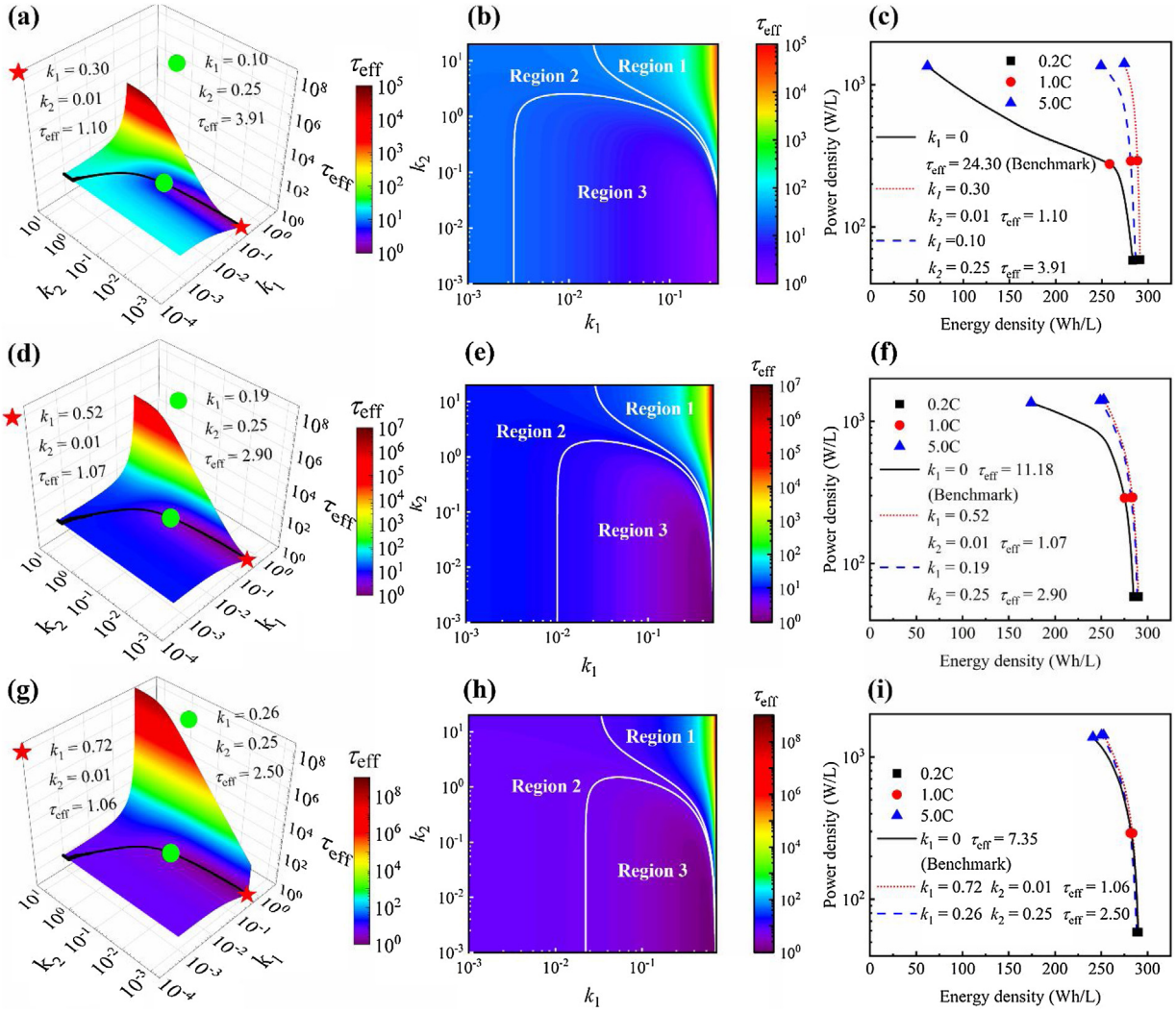

Fig. 5 – The effective tortuosity as a function of k_1 and k_2 at the total porosity of 0.25 (a), 0.35 (d), and 0.42 (g). The regions of the effective tortuosity at the total porosity of 0.25 (b), 0.35 (e), and 0.42 (h). The Ragone plots of the optimal electrode with $k_2 = 0.01$ and 0.25 as well as the benchmark electrode at the total porosity of 0.25 (c), 0.35 (f), and 0.42 (i). The black lines in Fig. 5a, d, and g show the minimum effective tortuosities when fixing k_2. In Fig. 5b, e, and h, Region 1 ($\tau_{eff} > 1.2\tau_B$, τ_B is the benchmark tortuosity), Region 2 ($0.8\tau_B \le \tau_{eff} \le 1.2\tau_B$), and Region 3 ($\tau_{eff} < 0.8\tau_B$) are labeled. Simulation parameters: $h = 60\,\mu m$, the other parameters are given in Table S1 in the Supplementary Information.

concentration drop in the electrode pillar along the y direction can be assumed to be negligible. Thus, in this limiting case, the effective tortuosity can be approximated by:

$$\tau_{eff} = \varepsilon \frac{1 + k_1}{k_1 + \varepsilon_e^m} \tag{23}$$

In case 2, the width of the electrode pillar or the ratio between the width and thickness of the electrode pillar is very large, and the concentration drop in the pore channel can be assumed to be negligible. In this limiting case, the effective tortuosity is approximated by:

$$\tau_{eff} = \varepsilon \frac{1 + k_1}{\varepsilon_e^m} \tag{24}$$

In case 3, the width of the electrode pillar is moderate, and all the concentration drops (i.e., Δc_{ex}, Δc_{ey}, and Δc_{pc}) are important. In this case, the effective tortuosity should be describe by Eq. (22). When k_1 is 0 (the conventional electrode with no cuboid pore channels), Eqs. (22)–(24) all turn into the Bruggeman equation that is used in the electrode pillar:

$$\tau_{eff} = \varepsilon_e^{1-m} \tag{25}$$

The conventional electrode ($k_1 = 0$) is taken as the benchmark, when optimizing the electrode with the hierarchical pore network.

In case 1 ($k_2 = 0.01$, $w_e = 0.6\,\mu m$), the τ_{eff} calculated by the approximate equation (Eq. (23)) is almost the same to the one determined by Eq. (22), when k_1 is in the range of 0–0.4 (see Fig. 2a). The τ_{eff} decreases from 11.2 to 1.3 with k_1 changing from 0 to 0.4, implying the electrode performance should be improved with a wide cuboid pore channel. To validate this relation between τ_{eff} and the electrode performance, the Ragone plots at $k_1 = 0$, 0.1, 0.2 and 0.4 are obtained from numerical simulations, as shown in Fig. 2b. At a low discharge rate (<2C), the power and energy densities at different k_1 are very close, because the ion diffusion limitation is not significant. At a large discharge rate (>2C) where the diffusion limitation becomes important, the energy density increases significantly with k_1 changing from 0 to 0.4. For example, at the discharge

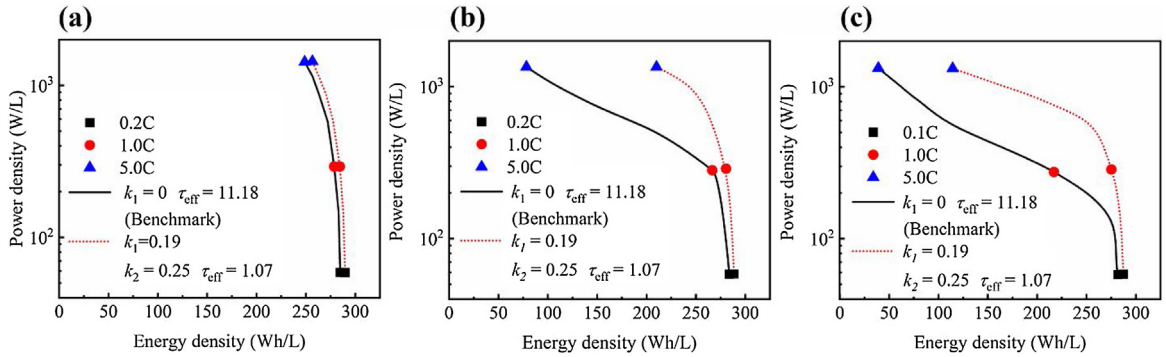

Fig. 6 – The Ragone plots of the optimal electrode with $k_2 = 0.25$ and the benchmark electrode at the electrode thickness of 30 μm (a), 90 μm (b), and 120 μm (c). Simulation parameters: $\varepsilon = 0.35$, the other parameters are given in Table S1 in the Supplementary Information.

rate of 10C, the energy density at $k_1 = 0.4$ (216 Wh/L) is 2.8 times larger than the benchmark (78 Wh/L). Therefore, the analytical method can be used to optimize the electrode with the hierarchical pore network in case 1. In this limiting case, the ion diffusion limitation in route 1 (see Fig. 1c) is very strong with a large k_1 due to the low porosity (see Eq. (11)), and route 2 becomes the primary route for ion transport. The cuboid pore channel in route 2 is the "high-way" for ion transport as its tortuosity is the minimum (i.e., 1). This explains the significant improvement of the electrode with the hierarchical pore network in this limiting case, when compared to the benchmark.

In case 2 ($k_2 = 20$, $w_e = 1200$ μm), the τ_{eff} determined by the approximate equation (Eq. (24)) is almost identical to the one obtained from Eq. (22) when k_1 is in the range of 0–0.4, as shown in Fig. 3a. The τ_{eff} increases with k_1, indicating the electrode performance would be reduced with a wide cuboid pore channel. The Ragone plots at $k_1 = 0$, 0.01, 0.1 and 0.15 are given in Fig. 3b. When the ion diffusion limitation is important (discharge rate >0.5C), the energy density decreases significantly when increasing k_1. For instance, at the discharge rate of 7C, the energy density at $k_1 = 0.15$ (29 Wh/L) is 78% lower than the benchmark (129 Wh/L). Thus, the analytical method is validated in case 2. In this limiting case, the ion diffusion limitation in route 2 (see Fig. 1c) is far stronger than that in route 1, and thus route 1 becomes the primary route for ion transport. As the porosity of the electrode pillar decreases with k_1 (see Eq. (11)) and its tortuosity increases with k_1 (see Eq. (25)), the electrode performance should be largely reduced with a wide cuboid pore channel, when compared to the benchmark.

In case 3 ($k_2 = 0.25$, $w_e = 15$ μm), there is a minimum τ_{eff} at $k_1 = 0.19$ (see Fig. 4a), suggesting that the electrode performance at $k_1 = 0.19$ is the best. To validate this result, the Ragone plots at $k_1 = 0$, 0.05, 0.19 and 0.4 are given in Fig. 4b. The energy density at $k_1 = 0.19$ is the highest, when the ion diffusion limitation is significant (discharge rate >1C). At the discharge rate of 10C, the energy density at $k_1 = 0.19$ (202 Wh/L) is 2.6 times as large as the benchmark (78 Wh/L). Hence, the analytical method is also valid in the case between the aforementioned two limiting cases. In this case, both route 1 and route 2 (see Fig. 1c) are important in transporting lithium ions. Introducing cuboid pore channels in the electrode can enhance or reduce the electrode performance, depending on the proportion of lithium ion transported in the cuboid pore channel (the "high-way" for ion transport) in route 2.

3.2. *Optimization at different total porosities*

Fig. 5a, d and g display the effective tortuosity (τ_{eff}) as a function of k_1 and k_2 at different total porosities (i.e., 0.25, 0.35, and 0.42), and these figures are used to optimize the electrode with the hierarchical pore network. The τ_{eff} can be divided into three regions, as seen in Fig. 5b, e and h. In region 1 where k_2 and k_1 are large, the τ_{eff} is higher than $1.2\tau_B$ (τ_B is the benchmark tortuosity), indicating the electrode performance can be largely reduced in this region. In region 2 where k_1 is small, the τ_{eff} is between $1.2\tau_B$ and $0.8\tau_B$, suggesting the performance of the electrode with the hierarchical pore network is close to the one of the conventional electrode in this region. In region 3 where k_2 is small but k_1 is large, the τ_{eff} is lower than $0.8\tau_B$, indicating the electrode performance can be significantly improved in this region. The areas the three regions change with the total porosity: the areas of region 1 and region 3 decreases with the total porosity, while the area of region 2 increases with the total porosity. When the total porosity is lower, the ion transport limitation is stronger, and thus the electrode performance is more sensitive to the structure change of the hierarchical pore network.

There is a minimum τ_{eff} that corresponds to an optimal k_1 when fixing k_2, and these minimum τ_{eff} are plotted in Fig. 5a, d and g. With a very small k_2, the optimal k_1 is the maximum value that k_1 can reach and the corresponding τ_{eff} is very close to 1; with a very large k_2, the optimal k_1 is 0 and the corresponding τ_{eff} is the same as the benchmark. According to Fig. 5a, d and g, an electrode with very slim electrode pillars and wide cuboid pore channels is favorable. In practice, the width of the electrode pillar is limited by the diameter of the electrode active material. In our simulations, the diameter of the electrode active material is 15 μm, and thus k_2 should be larger than 0.25. Fig. 5c, f and i give the Ragone plots of the optimal electrodes with $k_2 = 0.01$ and 0.25 at different total porosities (i.e., 0.25, 0.35, and 0.42). When the total porosity is 0.25, the optimal k_1 are 0.3 and 0.1 for $k_2 = 0.01$ and 0.25, and their corresponding τ_{eff} are 1.10 and 3.91. As the optimal electrode with $k_2 = 0.01$ has the τ_{eff} very close to the theoretical minimum (i.e., 1), this electrode can be regarded as the global optimum. At the discharge rate of 5C, the energy density of the optimal electrode with $k_2 = 0.01$ (274 Wh/L) is 10% higher than for the optimal electrode with $k_2 = 0.25$ (249 Wh/L) and 4.5 times larger than the benchmark (61 Wh/L). When the total porosity is 0.35, the Ragone plot for $k_2 = 0.01$ is close to the one for $k_2 = 0.25$, and the energy density of the optimal electrode

with $k_2 = 0.01$ (253 Wh/L) is 45% higher than the benchmark (174 Wh/L) at the discharge rate of 5C; when the total porosity is 0.42, the Ragone plot for $k_2 = 0.01$ is almost identical to the one for $k_2 = 0.25$, and the energy density of the optimal electrode with $k_2 = 0.01$ (253 Wh/L) is only 5% higher than the benchmark (241 Wh/L) at the discharge rate of 5C. For the electrode with a high total porosity, the ion diffusion limitation is not strong, and thus optimizing the hierarchical pore channel cannot lead to significant improvement in electrode performance.

3.3. *Optimization at different electrode thicknesses*

Fig. 6 displays the Ragone plots of the optimal electrode with $k_2 = 0.25$ and the benchmark electrode at different electrode thicknesses (i.e., 30, 90, and 120 μm). The effective tortuosity is independent on the electrode thickness according to Eq. (22), and it is displayed in Fig. 5d at the total porosity of 0.35. When the electrode thickness is 30 μm, the Ragone plot of the optimal electrode with $k_2 = 0.25$ is very close to the one of the benchmark electrode, as the ion diffusion limitation is negligible and introducing the cuboid pore channels would not improve the electrode performance. When the electrode thickness is 90 μm, the energy density of the optimal electrode with $k_2 = 0.25$ (210 Wh/L) is 2.7 times as high as the benchmark (78 Wh/L) at the discharge rate of 5C; when the electrode thickness is 120 μm, the energy density of the optimal electrode with $k_2 = 0.25$ (114 Wh/L) is 2.9 times as high as the benchmark (39 Wh/L) at the discharge rate of 5C. Therefore, introducing the cuboid pore channels can significantly enhance the electrode performance when the electrode is thick and the ion diffusion limitation is strong.

4. Conclusions

In this work, an analytical method is developed to optimize the lithium ion battery electrode with the hierarchical pore network, in which low-tortuosity cuboid pore channels are introduced into the conventional electrode as ion transport "high-way". The objective function is the analytical expression of the effective tortuosity that reflects the electrode performance, and the widths of the pore channel and electrode pillar are design variables.

With a commercial lithium-ion battery (UP 383562, Sony) as an example, the analytical method is validated in three archetypical cases (two limiting cases and one case between the two limiting cases), by comparing the analytical results with the numerical ones calculated by the Newman model. Using the analytical method, the electrode with the hierarchical pore network is optimized at different total porosities and electrode thicknesses. At a high total porosity (>0.42) and a low electrode thickness (<30 μm), introducing an optimal hierarchical pore network only slightly improves the electrode performance, as the ion transport limitation is not strong in these cases. At the low total porosity of 0.25, the optimal electrode with the hierarchical pore network can have an energy density 4.5 times as large as the benchmark; at the high electrode thickness of 120 μm, the optimal electrode with the hierarchical pore network can have an energy density 2.9 times as large as the benchmark. These results indicate properly engineering the hierarchical pore network in the electrode can significantly improve the electrode performance without changing its materials chemistry. The analytical method proposed in this work is simple yet effective, and should serve to design lithium ion battery electrodes with the hierarchical pore network.

Acknowledgments

This work was supported by the National Natural Science Foundation of China (21676082 and 21706067), the China Postdoctoral Science Foundation (2018T110358), the "Chenguang Program" supported by Shanghai Education Development Foundation and Shanghai Municipal Education Commission (17CG29), and the Fundamental Research Funds for the Central Universities (222201714004 and 222201718003).

Appendix A. Supplementary data

Supplementary material related to this article can be found, in the online version, at doi:https://doi.org/10.1016/j.cherd.2019.06.038.

References

Bae, C.J., Erdonmez, C.K., Halloran, J.W., Chiang, Y.M., 2013. Design of battery electrodes with dual-scale porosity to minimize tortuosity and maximize performance. Adv. Mater. 25, 1254–1258, http://dx.doi.org/10.1002/adma.201204055.

Billaud, J., Bouville, F., Magrini, T., Villevieille, C., Studart, A.R., 2016. Magnetically aligned graphite electrodes for high-rate performance Li-ion batteries. Nat. Energy 1, 1–6, http://dx.doi.org/10.1038/nenergy.2016.97.

Cobb, C.L., Blanco, M., 2014. Modeling mass and density distribution effects on the performance of co-extruded electrodes for high energy density lithium-ion batteries. J. Power Sources 249, 357–366, http://dx.doi.org/10.1016/j.jpowsour.2013.10.084.

Coppens, M.O., Ye, G., 2018. Nature-inspired optimization of transport in porous media. In: Bunde, A., Caro, J., Kärger, J., Gero, V. (Eds.), Diffusive Spreading in Nature, Technology and Society. Springer, Cham, pp. 203–232, http://dx.doi.org/10.1007/978-3-319-67798-9_11.

Dai, Y., Srinivasan, V., 2016. On graded electrode porosity as a design tool for improving the energy density of batteries. J. Electrochem. Soc. 163, A406–A416, http://dx.doi.org/10.1149/2.0301603jes.

Doyle, M., Fuentes, Y., 2003. Computer simulations of a lithium-ion polymer battery and implications for higher capacity next-generation battery designs. J. Electrochem. Soc. 150, A706–A713, http://dx.doi.org/10.1149/1.1569478.

Doyle, M., Fuller, T.F., Newman, J., 1993. Modeling of galvanostatic charge and discharge of the lithium/polymer/insertion cell. J. Electrochem. Soc. 140, 1526–1533.

Doyle, M., Newman, J., 1997. Analysis of capacity–rate data for lithium batteries using simplified models of the discharge process. J. Appl. Electrochem. 27, 846–856.

Etacheri, V., Marom, R., Elazari, R., Salitra, G., Aurbach, D., 2011. Challenges in the development of advanced Li-ion batteries: a review. Energy Environ. Sci. 4, 3243–3262, http://dx.doi.org/10.1039/c1ee01598b.

Fuller, T.F., Doyle, M., Newman, J., 1994. Simulation and optimization of the dual Lithium ion insertion cell. J. Electrochem. Soc. 141, 1–10, http://dx.doi.org/10.1149/1.2054684.

Golmon, S., Maute, K., Dunn, M.L., 2014. A design optimization methodology for Li+ batteries. J. Power Sources 253, 239–250, http://dx.doi.org/10.1016/j.jpowsour.2013.12.025.

Hutzenlaub, T., Asthana, A., Becker, J., Wheeler, D.R., Zengerle, R., Thiele, S., 2013. FIB/SEM-based calculation of tortuosity in a porous LiCoO2 cathode for a Li-ion battery. Electrochem. commun. 27, 77–80, http://dx.doi.org/10.1016/j.elecom.2012.11.006.

Kang, B., Ceder, G., 2009. Battery materials for ultrafast charging and discharging. Nature 458, 190–193, http://dx.doi.org/10.1038/nature07853.
Long, J.W., Dunn, B., Rolison, D.R., White, H.S., 2004. Three-dimensional battery architectures. Chem. Rev. 104, 4463–4492, http://dx.doi.org/10.1021/cr020740l.
Lueth, S., Sauter, U.S., Bessler, W.G., 2016. An agglomerate model of lithium-ion battery cathodes. J. Electrochem. Soc. 163, A210–A222, http://dx.doi.org/10.1149/2.0291602jes.
Miranda, D., Costa, C.M., Almeida, A.M., Lanceros-Méndez, S., 2016. Computer simulations of the influence of geometry in the performance of conventional and unconventional lithium-ion batteries. Appl. Energy 165, 318–328, http://dx.doi.org/10.1016/j.apenergy.2015.12.068.
Newman, J., 1995. Optimization of porosity and thickness of a battery electrode by means of a reaction-zone model. J. Electrochem. Soc. 142, 97–101, http://dx.doi.org/10.1149/1.2043956.
Nitta, N., Wu, F., Lee, J.T., Yushin, G., 2015. Li-ion battery materials: present and future. Mater. Today 18, 252–264, http://dx.doi.org/10.1016/j.mattod.2014.10.040.
Palacín, M.R., 2009. Recent advances in rechargeable battery materials: a chemist's perspective. Chem. Soc. Rev. 38, 2565–2575, http://dx.doi.org/10.1039/b820555h.
Park, M., Zhang, X., Chung, M., Less, G.B., Sastry, A.M., 2010. A review of conduction phenomena in Li-ion batteries. J. Power Sources 195, 7904–7929, http://dx.doi.org/10.1016/j.jpowsour.2010.06.060.
Pikul, J.H., Zhang, H.-G., Cho, J., Braun, P.V., King, W.P., 2013. High-power lithium ion microbatteries from interdigitated three-dimensional bicontinuous nanoporous electrodes. Nat. Commun. 4, 1732–1735, http://dx.doi.org/10.1038/ncomms2747.
Ramadesigan, V., Methekar, R.N., Latinwo, F., Braatz, R.D., Subramanian, V.R., 2010. Optimal porosity distribution for minimized ohmic drop across a porous electrode. J. Electrochem. Soc. 157, A1328–A1334, http://dx.doi.org/10.1149/1.3495992.
Rao, S.M., Coppens, M.-O., 2010. Mitigating deactivation effects through rational design of hierarchically structured catalysts: application to hydrodemetalation. Ind. Eng. Chem. Res. 49, 11087–11097, http://dx.doi.org/10.1021/ie1009487.
Richardson, G., Denuault, G., Please, C.P., 2012. Multiscale modelling and analysis of lithium-ion battery charge and discharge. J. Eng. Math. 72, 41–72, http://dx.doi.org/10.1007/s10665-011-9461-9.
Sander, J.S., Erb, R.M., Li, L., Gurijala, A., Chiang, Y.M., 2016. High-performance battery electrodes via magnetic templating. Nat. Energy 1, 1–7, http://dx.doi.org/10.1038/nenergy.2016.99.
Schwieger, W., Machoke, A.G., Weissenberger, T., Inayat, A., Selvam, T., Klumpp, M., Inayat, A., 2016. Hierarchy concepts: classification and preparation strategies for zeolite containing materials with hierarchical porosity. Chem. Soc. Rev. 45, 3353–3376, http://dx.doi.org/10.1039/C5CS00599J.
Srinivasan, V., Newman, J., 2004. Design and optimization of a natural Graphite/Iron phosphate lithium-ion cell. J. Electrochem. Soc. 151, A1530, http://dx.doi.org/10.1149/1.1785013.
Subramanian, V.R., White, R.E., 2000. A semianalytical method for predicting primary and secondary current density distributions: linear and nonlinear boundary conditions. J. Electrochem. Soc. 147, 1636–1644, http://dx.doi.org/10.1149/1.1393410.
Wang, G., Johannessen, E., Kleijn, C.R., de Leeuw, S.W., Coppens, M.-O., 2007. Optimizing transport in nanostructured catalysts: a computational study. Chem. Eng. Sci. 62, 5110–5116, http://dx.doi.org/10.1016/j.ces.2007.01.046.
Ye, G., Duan, X., Zhu, K., Zhou, X., Coppens, M.-O., Yuan, W., 2015. Optimizing spatial pore-size and porosity distributions of adsorbents for enhanced adsorption and desorption performance. Chem. Eng. Sci. 132, 108–117, http://dx.doi.org/10.1016/j.ces.2015.04.024.
Zhang, Q., White, R.E., 2007. Comparison of approximate solution methods for the solid phase diffusion equation in a porous electrode model. J. Power Sources 165, 880–886, http://dx.doi.org/10.1016/j.jpowsour.2006.12.056.